arXiv:1209.5624v1 [physics.atom-ph] 25 Sep 2012

Measuring the atomic recoil frequency using a perturbative grating-echo atom interferometer

B. Barrett,* A. Carew, S. Beattie,† and A. Kumarakrishnan
Department of Physics & Astronomy, York University, Toronto, Ontario M3J 1P3, Canada

(Dated: September 26, 2012)

We describe progress toward a precise measurement of the recoil energy of an atom measured using a unique perturbative grating-echo atom interferometer (AI) that involves three standing-wave (sw) pulses. Experiments are performed using samples of laser-cooled rubidium atoms with temperatures $< 5\ \mu$K in a non-magnetic apparatus. The AI signal exhibits narrow fringes that revive periodically at the two-photon recoil frequency, ω_q, as a function of the third sw pulse time. Using this technique, we demonstrate a measurement of ω_q with a statistical uncertainty of 37 parts per 10^9 (ppb) on a time scale of ~ 45 ms in 14 hours. Further statistical improvements are anticipated by extending this time scale and narrowing the signal fringe width. However, the estimated systematic uncertainty is ~ 6 parts per 10^6 (ppm). We describe methods of reducing these systematic errors to competitive levels.

There is an ongoing, international effort to develop precise, independent techniques for measuring the atomic fine structure constant, α—a dimensionless parameter that quantifies the strength of the electromagnetic force. These measurements can be used to stringently test the theory of quantum electrodynamics (QED). Historically, two types of determinations of α have been carried out: (i) those that use another precisely measured quantity, such as the magnetic moment of the electron, to determine α through challenging QED calculations [1, 2], and (ii) those that are independent of QED. The latter depend on only the quantities appearing in the definition $\alpha \equiv e^2/2\epsilon_0 hc$, where e is the elementary charge, ϵ_0 is the vacuum permittivity, h is Planck's constant and c is the speed of light. Some examples of α determinations that require QED are the precise measurements of the anomalous magnetic moment of the electron [3], and the fine structure intervals of helium [4]. The most precise examples of QED-independent determinations are those based on measurements of the von Klitzing constant, $R_{\rm K} = h/e^2$, using the quantum-Hall effect [5, 6], and those based on measurements of the ratio h/M using (i) Bloch oscillations in cold atoms [7] and (ii) atom interferometric techniques [8–11]. Other techniques that show high sensitivity to h/M include Refs. [12, 13]. Within these examples, atom interferometry has emerged as a powerful tool because of its inherently high sensitivity to h/M, which can be related to α according to

$$\alpha^2 = \frac{2R_\infty}{c}\frac{h}{m_e} = \frac{2R_\infty}{c}\left(\frac{M}{m_e}\right)\left(\frac{h}{M}\right). \tag{1}$$

Here, R_∞ is the Rydberg constant, m_e is the electron mass, and M is the mass of the test atom. Since R_∞ is known to 5 parts in 10^{12}, and the mass ratio M/m_e is typically known to a few parts in 10^{10} [14], the quantity that limits the precision of a determination of α using Eq. (1) is the ratio h/M. Currently, the best measurement of this ratio was recently carried out in ^{87}Rb, where $h/M(^{87}\text{Rb})$ was determined to 1.2 ppb [11].

The focus of this work is a precise determination of α from the ratio $h/M_{\rm Rb}$ using a unique three-pulse perturbative grating-echo AI. In recent years, the grating-echo AI has emerged as a candidate for precise measurements of the two-photon recoil frequency, $\omega_q = \hbar q^2/2M$, where $\hbar q = 2\hbar k$ is the two-photon momentum and k is the wave number of the light [15]. The appeal of this AI lies in its reduced experimental complexity compared to Raman AIs (i.e. it does not require internal state or velocity selection, and it utilizes only one excitation frequency). Additionally, since this interferometer uses only one hyperfine ground state, it has reduced sensitivity to common systematic effects such as the ac Stark and Zeeman shifts. Phase noise in the excitation beams due to mirror vibrations is also a negligible concern with this interferometer, since the excitation pulses are short-lived ($\lesssim 1$ μs) and the interference can be probed using intensity detection.

The principles of the grating-echo AI can be understood on the basis of a plane-wave description as shown in Fig. 1(a) [15–19]. The AI relies on Kapitza-Dirac scattering of atoms by short, off-resonant sw pulses. Two sw pulses, spaced in time by T, are applied to a sub-Doppler laser-cooled sample with a root-mean-squared (rms) momentum spread of $p_{\rm rms} = (Mk_B\mathcal{T})^{1/2} \gg \hbar k$, where $\mathcal{T}$ is the sample temperature and k_B is Boltzmann's constant. For each atom in the sample, the first pulse excites a superposition of momentum states separated by integer multiples of $\hbar q$. Between the pulses, the wave function associated with each momentum state develops a time-dependent phase $\phi(t) = (p_0 + n\hbar q)^2 t/2M\hbar$ due to its kinetic energy, where p_0 is the initial momentum of the atom and n is an integer. The second excitation pulse further diffracts the momentum states, causing certain trajectories to interfere in the vicinity of $t = 2T$. This interference creates a spatial modulation in the atomic probability density. At the "echo" time, $t = 2T$, the contribution to the phase modulation of wave function due to p_0 (i.e. the Doppler phase, $\phi_D(t) = nqv_0t$, where

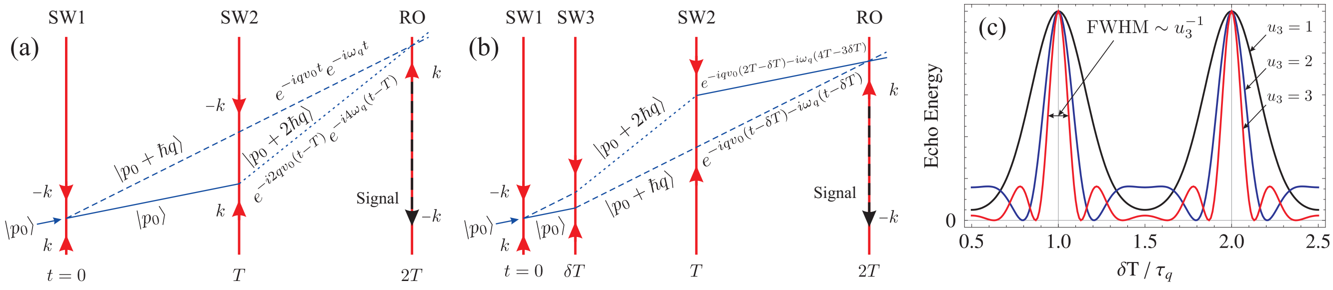

FIG. 1. (Color online) (a) Lowest-order momentum trajectories for the two-pulse AI. The Doppler phase contribution to the interference between the two trajectories, $qv_0(t - 2T)$, is zero at the echo time, $t = 2T$, for all initial atomic velocities, $v_0 = p_0/M$. (SW1 = first sw pulse, RO = read-out pulse) (b) Example of low-order momentum trajectories for the three-pulse perturbative AI. Here, the Doppler phase contribution is zero at $t = 2T$ and independent of δT for only those trajectories that differ by $\hbar q$ after SW3. (c) Echo energy as a function of $\delta T/\tau_q$, where $\tau_q = \pi/\omega_q$ is the recoil period. Line shapes are shown for three different pulse areas, u_3, assuming only one magnetic sub-level contributes to the signal and that spatial profile effects associated with the excitation beams are negligible.

$v_0 = p_0/M$), is equal for two interfering trajectories. Here, we have ignored the $p_0^2 t/2M\hbar$ term that is common to all trajectories and is not important for interference. Thus, for all velocity classes, the Doppler phase cancels between interfering momentum states—resulting in a macroscopic density grating that remains coherent for a time $\tau_{\mathrm{coh}} \sim M/(n - n')qp_{\mathrm{rms}}$ about $t = 2T$. Here, n and $n' \neq n$ are integers representing separate interfering momentum states. The remaining phase component due to the recoil of the atom, $\phi_q(t) = n^2\omega_q t$, is, in general, non-zero at the echo time and oscillates at an integer multiple of ω_q. An example of two interfering trajectories for low-order momentum states is shown in Fig. 1(a).

The grating contrast is measured by applying a traveling-wave read-out pulse and detecting the intensity of the coherently Bragg-scattered light from the atomic cloud in the backward direction. Due to the nature of Bragg diffraction, this detection technique is sensitive to only the harmonics of the density modulation that have a period $m\lambda/2$, where m is an integer. In the plane-wave picture, only interfering momentum states that differ by $\hbar q$ can produce such a modulation. The time-integrated power of the back-scattered light (referred to as the echo energy) is a measure of the grating contrast produced by this interference. Experiments utilizing the two-pulse AI, where the echo energy is measured as a function of T, are described in Refs. [15–18].

For the three-pulse perturbative AI, an additional sw pulse is applied between the first two pulses at $t = \delta T < T$, as shown in Fig. 1(b) [20]. This pulse has the effect of diffracting the atom into higher-order momentum states that contribute additional harmonics to the recoil modulation of the grating contrast. However, only a small subset of the excited trajectories will interfere at the echo time for an arbitrary δT (i.e. trajectories which, when combined, exhibit a Doppler phase that is independent of δT). Specifically, the only momentum states contributing to the signal are those that differ by $\hbar q$ after SW3 *and* after SW2, as shown by the example in Fig. 1(b). When all possible trajectories are summed over, it can be shown that the resulting echo energy is modulated by $J_0[2u_3 \sin(\omega_q \delta T)]^2$, provided the third pulse area is small (i.e. $u_3 = \Omega_0^2\tau_3/2|\Delta| \lesssim 1$) [21, 22]. Here, $J_0(x)$ is a Bessel function, Ω_0 is the one-photon Rabi frequency, τ_3 is the third sw pulse duration, and Δ is the detuning from the excited state. Figure 1(c) illustrates the predicted dependence of the echo energy (for a *single* ground state magnetic sub-level) as a function of δT. For small pulse durations [i.e. $\tau_3 \ll (|\Delta|/\Omega_0^2\omega_k)^{1/2}$, where $\omega_k = \hbar k^2/2M$], the full-width at half-maximum (FWHM) of the signal scales inversely with u_3. For this AI, the sensitivity to h/M scales with the width of the excited momentum distribution and inversely with the time scale (T) over which the signal can be measured.

As described in Refs. [19, 22], two major improvements to the grating-echo AI experiment have enabled us to reach time scales of $T \sim 50$ ms: (i) utilizing a non-magnetizable glass vacuum system, which reduced decoherence effects related to B-field gradients and improved the molasses cooling of the sample, and (ii) using large-diameter chirped excitation beams, which eliminated the differential Doppler shift between the two components of the sw pulses.

The experiment utilizes a laser-cooled sample of rubidium typically containing $\sim 5 \times 10^9$ atoms at temperatures of $\mathcal{T} \lesssim 5\ \mu$K. Either ^{85}Rb or ^{87}Rb atoms are loaded into a magneto-optical trap (MOT) from a background Rb vapor. Before the AI experiment, the sample is prepared in the upper hyperfine atomic ground state (5S$_{1/2}$ $F = 3$ for ^{85}Rb or $F = 2$ for ^{87}Rb). The light for the AI is derived from a Ti:sapphire laser (linewidth ~ 1 MHz) that is locked above the D2 cycling transition using Doppler-free saturated absorption spectroscopy. A network of acousto-optic modulators (AOMs) is used to generate the frequencies necessary for the AI excitation and the read-out beams. The read-out light is detuned

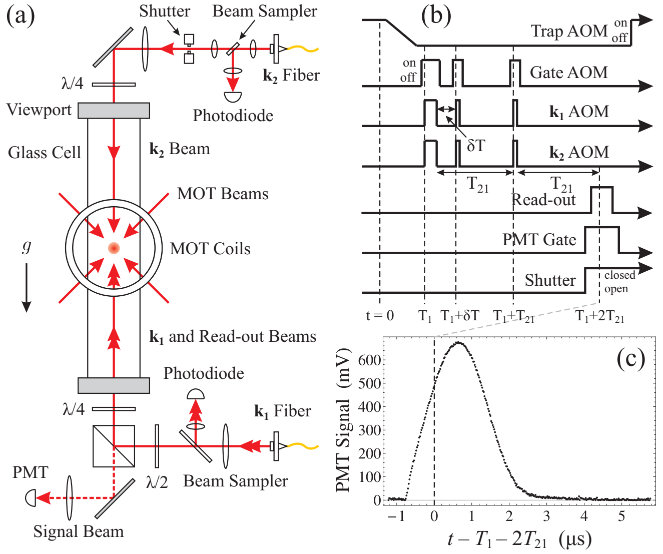

FIG. 2. (Color online) (a) Optical setup for the interferometer. The glass cell has dimensions 7.6 × 7.6 × 84 cm and is oriented along the vertical. (b) Timing diagram for the AI. The gate AOM is pulsed on to allow light for each excitation pulse produced by the k_1 and k_2 AOMs, where three pulses are shown. The pulse occurring at $t = T_1 + \delta T$ corresponds to the perturbative sw pulse. The read-out pulse (which is independent of the gate AOM) and the PMT gate are turned on for ~ 9 μs in the vicinity of the echo time, $t = T_1 + 2T_{21}$. (c) Example of a two-pulse grating-echo signal (from a 10 μK ^{87}Rb sample) recorded by the PMT, which corresponds to an echo energy of 130 pJ. AI pulse parameters: $T_{21} = 1.06338$ ms, $\tau_1 = 3.8$ μs, $\tau_2 = 1.2$ μs, $\Delta_{\rm AI} = 220$ MHz, $\Delta_{\rm RO} = 40$ MHz, $I_{\rm AI} = I_{\rm RO} \sim 43$ mW/cm^2, $d_{\rm AI} \sim 1.7$ cm.

by $\Delta_{\rm RO} = 40$ MHz from the cycling transition—a condition that increases the back-scattered light intensity from the atoms [22]. The AI beams are detuned by $\Delta_{\rm AI} = 220$ MHz, and a frequency chirp of $\delta(t) = gt/\lambda$ is added to (subtracted from) the downward traveling (upward traveling) component of the sw pulses such that each excitation is kept on resonance with the two-photon transition [19, 22]. Here, g is the gravitational acceleration, and λ is the wavelength of the AI light. A "gate" AOM is used upstream of the AI AOMs as a frequency shifter and as a high-speed shutter to reduce the amount of stray light in the experiment. All rf sources and digital-delay generators used to define the pulse timing for the AI are externally referenced to a 10 MHz rubidium clock.

The AI beams are coupled into two AR-coated single-mode optical fibers and aligned through the sample, as shown in Fig. 2(a). At the output of the fibers, the beams are expanded to a e^{-1} diameter of $d_{\rm AI} \sim 1.7$ cm and are circularly polarized in the same manner by a pair of $\lambda/4$ wave plates. The timing sequence for the experiment is illustrated in Fig. 2(b). A mechanical shutter on the upper platform closes just before the read-out pulse is applied to block any optical back-scattering of read-out light from interfering with the signal from the atoms. A gated photo-multiplier tube (PMT) is used to detect the power in the echo signal. Fig. 2(c) shows an example of the back-scattered echo signal from the two-pulse AI.

Measurements of ω_q were obtained using the perturbative three-pulse AI by measuring the echo energy as a function of the third sw pulse time, $T_3 = T_1 + \delta T$, as shown in Fig. 3(a). Here, $\delta T < T_{21} = T_2 - T_1$. To measure ω_q, data are fit to a phenomenological model that consists of a periodic sum of exponentially-modified Gaussian functions, and the recoil frequency is extracted from the fit. Figure 3(a) shows a measurement of ω_q in ^{85}Rb on a time scale of $T_{21} \sim 36.7$ ms that was acquired in ~ 15 minutes. The fit to these data yields a statistical precision of $\delta\omega_q/\omega_q \sim 180$ ppb. This represents a factor of ~ 9 improvement over previous work [20].

To demonstrate the statistical uncertainty of the measurement under current conditions, 82 independent measurements of ω_q in ^{87}Rb were obtained with all other experimental conditions held fixed to the extent possible. The distribution of individual recoil measurements is shown in Fig. 3(b). Here, ω_q is determined from a weighted average over all individual measurements, where the points are weighted inversely proportional to the square of their statistical uncertainties. The mean value, which has not been corrected for systematic effects, is found with a relative statistical uncertainty of 37 ppb as determined by the standard deviation of the mean. An autocorrelation analysis of the measurements shown in Fig. 3(b) indicates that the results are correlated at the 20% level with measurements taken at a previous time. This is attributed to slowly varying lab conditions over the 14 hours of data acquisition time. The primary contributors to these correlations are the temperature and the time-varying ambient magnetic environment of the lab, which are currently being stabilized for a new round of measurements.

We have investigated systematic effects on the measurement of ω_q related to the angle between excitation beams, the refractive indices of the sample and the background Rb vapor, light shifts, Zeeman shifts, B-field curvature and the sw pulse durations [22]. The total systematic uncertainty in this measurement is estimated to be ~ 5.7 ppm, and is dominated by two effects: (i) the refractive index of the sample, and (ii) the curvature of the B-field that the atoms experience as they fall under gravity. For our sample density ($\sim 4 \times 10^{10}$ atom/cm^3) and detuning ($\Delta_{\rm AI} = 219.8$ MHz), we estimate a shift in ω_q of $-10.5(3.0)$ ppm based on Ref. [24]. Similarly, independent studies of the B-field curvature (~ 0.4 mG/cm^2) indicate a shift of $+6.3(4.4)$ ppm [22].

The systematic shift due to the B-field curvature can be significantly reduced by selecting only the $m_F = 0$ atoms using a microwave π-pulse and a bias B-field. This will have the added benefit of eliminating decoherence due to this curvature—enabling an increase in T_{21}

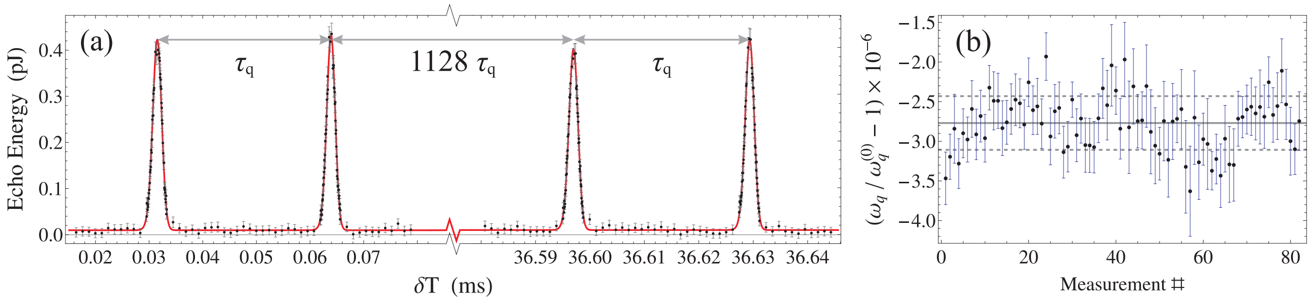

FIG. 3. (Color online) (a) Demonstration of an individual recoil measurement in ^{85}Rb using the perturbative AI at $T_{21} = 36.6656$ ms. Data are recorded in two temporal windows separated by $1128\,\tau_q \sim 36.5$ ms. The relative statistical uncertainty in ω_q is ~ 180 ppb, as determined from a non-linear least-squares fit. (b) 82 independent measurements of ω_q in ^{87}Rb displayed in chronological order. Each data point was recorded in $\sim$ 10 minutes of data acquisition time, with a typical statistical uncertainty of ~ 380 ppb. Measurements are scaled by the expected value of the recoil frequency, $\omega_q^{(0)} = 94.77384783(12)$ rad/ms, which is based on the value of $h/M(^{87}\text{Rb})$ from Ref. [11] and the $F = 2 \rightarrow F' = 3$ transition frequency in ^{87}Rb from Ref. [23]. The dashed grid lines indicate the weighted standard deviation of 339 ppb, and the standard deviation of the mean is 37 ppb. The corresponding reduced chi-squared is $\chi^2/\text{dof} = 0.93$ for dof = 81 degrees of freedom. The mean value, shown by the solid grid line, is ~ 2.8 ppm below the expected value, which is due to systematic effects. AI pulse parameters: $T_{21} = 45.4837$ ms, $\tau_1 = 2.2$ μs, $\tau_2 = 1.4$ μs, $\tau_3 = 3$ μs, $\Delta_{\text{AI}} = 219.8$ MHz, $\Delta_{\text{RO}} \sim 40$ MHz, $I_{\text{AI}} = I_{\text{RO}} \sim 96$ mW/cm^2, $d_{\text{AI}} \sim 1.7$ cm.

and a corresponding reduction in the statistical error of each measurement. Under current conditions, we have achieved a maximum time scale of $T_{21} \sim 65$ ms. However, previous studies indicate that the transit time of the atoms in the excitation beams is ~ 270 ms [19], suggesting that T_{21} can be as large as ~ 135 ms before the temperature of the sample becomes the limiting factor. The systematic shift due to the refractive index of the sample can be reduced by decreasing the sample density, or increasing the detuning of the AI beams. However, the current configuration of the AI requires a large number of atoms in order to achieve a sufficient signal-to-noise ratio. Also, the sensitivity of the three-pulse perturbative AI relies on a relatively strong atom-field coupling in order to excite many orders of momentum states. Thus, a decrease in the sample density or an increase in the excitation beam detuning both lead to a reduction in the signal size and, therefore, in the sensitivity of the AI to ω_q. A possible method of addressing this challenge is to increase the intensity of the backscattered signal by pre-loading the sample in an optical lattice such that the initial spatial distribution has a significant $\lambda/2$-periodic component [25]. Experimental studies of MOTs loaded into an intense, off-resonant optical lattice has shown that the reflection coefficient of the light that is Bragg-scattered off the resulting atomic grating can be as large as $R \sim 0.8$ [26], whereas we estimate $R \sim 0.001$ for the grating-echo in this work. This motivates the pursuit of high-contrast grating-echo production in order to increase the signal-to-noise ratio in the experiment. Such a procedure may then allow the density of the sample to be reduced (by tailoring the selection of $m_F = 0$ atoms to yield low numbers) while retaining sufficient signal-to-noise. Additionally, by using the intense lattice beam to generate the excitation pulses required for the AI, the width of the recoil fringes can be further reduced—thereby improving the statistical uncertainty of each measurement. With these experimental improvements, we anticipate that a future round of measurements will yield results with both statistical and systematic uncertainties at competitive levels.

This work was supported by the Canada Foundation for Innovation, Ontario Innovation Trust, the Natural Sciences and Engineering Research Council of Canada, Ontario Centres of Excellence, the US Army Research Office and York University. We thank Tycho Sleator of New York University for lending crucial components of a Ti:sapphire laser.

---

[*] Current address: Laboratoire Photonique Numérique et Nanosciences, Université Bordeaux 1, IOGS and CNRS, 351 cours de la Libération, 33405 Talence, France

[†] Current address: Department of Physics, University of Toronto, Toronto, Ontario M5S 1A7, Canada

[1] T. Aoyama, M. Hayakawa, T. Kinoshita, and M. Nio, Phys. Rev. Lett. **99**, 110406 (2007).
[2] K. Pachucki, V. A. Yerokhin, and P. Cancio Pastor, Phys. Rev. A **85**, 042517 (2012).
[3] D. Hanneke, S. Fogwell, and G. Gabrielse, Phys. Rev. Lett. **100**, 120801 (2008).
[4] M. Smiciklas and D. Shiner, Phys. Rev. Lett. **105**, 123001 (2010).
[5] A.-M. Jeffery, R. E. Elmquist, L. H. Lee, J. Q. Shields, and R. F. Dziuba, IEEE Trans. Instrum. Meas. **46**, 264 (1997).
[6] G. W. Small, B. W. Ricketts, P. C. Coogan, B. J. Pritchard, and M. M. R. Sovierzoski, Metrologia **34**,

241 (1997).
[7] P. Cladé, E. de Mirandes, M. Cadoret, S. Guellati-Khélifa, C. Schwob, F. Nez, L. Julien, and F. Biraben, Phys. Rev. Lett. **96**, 033001 (2006).
[8] D. S. Weiss, B. C. Young, and S. Chu, Phys. Rev. Lett. **70**, 2706 (1993).
[9] A. Wicht, J. M. Hensley, E. Sarajlic, and S. Chu, Phys. Scr. **T102**, 82 (2002).
[10] M. Cadoret, E. de Mirandes, P. Cladé, S. Guellati-Khélifa, C. Schwob, F. Nez, L. Julien, and F. Biraben, Phys. Rev. Lett. **101**, 230801 (2008).
[11] R. Bouchendira, P. Clade, S. Guellati-Khélifa, F. Nez, and F. Biraben, Phys. Rev. Lett. **106**, 080801 (2011).
[12] S. W. Chiow, S. Herrmann, S. Chu, and H. Müller, Phys. Rev. Lett. **103**, 050402 (2009).
[13] S. W. Chiow, T. Kovachy, H.-C. Chien, and M. A. Kasevich, Phys. Rev. Lett. **107**, 130403 (2011).
[14] P. J. Mohr, B. N. Taylor, and D. B. Newell, "CODATA recommended values of the fundamental physical constants: 2010," (2012), arXiv:1203.5425v1 [physics.atom-ph].
[15] S. B. Cahn, A. Kumarakrishnan, U. Shim, T. Sleator, P. R. Berman, and B. Dubetsky, Phys. Rev. Lett. **79**, 784 (1997).
[16] D. V. Strekalov, A. Turlapov, A. Kumarakrishnan, and T. Sleator, Phys. Rev. A **66**, 023601 (2002).
[17] S. Beattie, B. Barrett, M. Weel, I. Chan, C. Mok, S. B. Cahn, and A. Kumarakrishnan, Phys. Rev. A **77**, 013610 (2008).
[18] B. Barrett, I. Yavin, S. Beattie, and A. Kumarakrishnan, Phys. Rev. A **82**, 023625 (2010).
[19] B. Barrett, I. Chan, and A. Kumarakrishnan, Phys. Rev. A **84**, 063623 (2011).
[20] S. Beattie, B. Barrett, I. Chan, C. Mok, I. Yavin, and A. Kumarakrishnan, Phys. Rev. A **79**, 021605(R) (2009).
[21] S. Beattie, B. Barrett, I. Chan, C. Mok, I. Yavin, and A. Kumarakrishnan, Phys. Rev. A **80**, 013618 (2009).
[22] B. Barrett, *Techniques for measuring the atomic recoil frequency using a grating-echo atom interferometer*, Ph.D. thesis, York University (2012).
[23] D. A. Steck, "Rubidium 87 D Line Data," (revision 2.1.4, 23 December 2010), available online at steck.us/alkalidata.
[24] G. K. Campbell, A. E. Leanhardt, J. Mun, M. Boyd, E. W. Streed, W. Ketterle, and D. E. Pritchard, Phys. Rev. Lett. **94**, 170403 (2005).
[25] M. F. Andersen and T. Sleator, Phys. Rev. Lett. **103**, 070402 (2009).
[26] A. Schilke, C. Zimmermann, P. W. Courteille, and W. Guerin, Phys. Rev. Lett. **106**, 223903 (2011).